Monthly Notices
of the
ROYAL ASTRONOMICAL SOCIETY

Mon. Not. R. Astron. Soc. **401,** 1500–1504 (2010) doi:10.1111/j.1365-2966.2009.15769.x

Inverse-Compton X-rays from giant radio galaxies at $z \sim 1$

T. Laskar,[1,2⋆] A. C. Fabian,[1] K. M. Blundell[3] and M. C. Erlund[1]

[1] *Institute of Astronomy, Madingley Road, Cambridge CB3 0HA*
[2] *Trinity College, University of Cambridge, Cambridge CB2 1TQ*
[3] *University of Oxford, Astrophysics, Keble Road, Oxford OX1 3RH*

Accepted 2009 September 23. Received 2009 September 15; in original form 2009 May 15

ABSTRACT

We report *XMM–Newton* observations of three FR II radio galaxies at redshifts between 0.85 and 1.34, which show extended diffuse X-ray emission within the radio lobes, likely due to inverse-Compton up-scattering of the cosmic microwave background. Under this assumption, through spectrum fitting together with archival Very Large Array radio observations, we derive an independent estimate of the magnetic field in the radio lobes of 3C 469.1 and compare it with the equipartition value. We find concordance between these two estimates as long as the turnover in the energy distribution of the particles occurs at a Lorentz factor in excess of ∼250. We determine the total energy in relativistic particles in the radio-emitting lobes of all three sources to range between 3×10^{59} and 8×10^{59} erg. The nuclei of these X-ray sources are heavily-absorbed powerful active galactic nuclei.

Key words: galaxies: high-redshift – galaxies: jets – X-rays: galaxies – X-rays: individual (3C 469.1, MRC 2216−206, MRC 0947−249).

1 INTRODUCTION

Emission from inverse-Compton-scattered cosmic microwave background (CMB) (ICCMB) photons, in the form of diffuse, extended X-rays between the nucleus and radio hotspots, has been detected in a number of radio galaxies at cosmological distances (e.g. Fabian et al. 2003; Blundell et al. 2006; Johnson et al. 2007; Erlund, Fabian & Blundell 2008) and at low redshift (e.g. Croston et al. 2005). The ICCMB is a tracer of old, spent synchrotron plasma, and its usefulness as a diagnostic of the magnetic field and electron energy distribution in active galactic nuclei (AGN) lobes stems from the fact that it is not redshift-dimmed (Schwartz 2002), unlike other sources of continuum X-ray emission.

Together with radio observations, ICCMB X-ray fluxes can be used to constrain the local magnetic field experienced by the radio-emitting plasma in the lobes of giant FR II (Fanaroff & Riley 1974) radio sources (see e.g. Erlund et al. 2006). Previous observations of ICCMB X-rays from radio galaxies have found deviations of the observed magnetic field from predictions based on equipartition arguments (see Croston et al. 2005, and references therein). While this can be resolved if the energy distribution turns over at the low-energy end (Blundell et al. 2006) at relatively high Lorentz factors ($\gamma_{\rm min} \sim 10^3$), estimates of the low-energy turnover of the electron distribution in all observed radio galaxies and quasars have been largely inconclusive, with no consistent picture amongst the entire population of radio sources having yet emerged.

We present *XMM–Newton* observations of the FR II radio galaxy 3C 469.1, where we have detected extended X-ray emission, which is likely the ICCMB. We extract and fit the X-ray spectrum for this source and show the photon spectral index, Γ, to lie between 0.9 and 2.1, consistent with the radio synchrotron spectral index of 1.97 determined from NASA/IPAC Extragalactic Database (NED)[1] archival radio photometry. We use the calculated unabsorbed X-ray luminosity along with a new look at archival 1.5 GHz Very Large Array (VLA) data for this source to constrain the magnetic field, *without* assumptions of equipartition. Finally, we present X-ray observations of two more giant radio galaxies, MRC 2216−206 and MRC 0947−249, where ICCMB emission seems to be also apparent.

3C 469.1, MRC 2216−206 and MRC 0947−249 are located at redshifts of 1.336, 1.148 and 0.854, respectively, corresponding to linear scales of 8.6, 8.4 and 7.8 kpc/arcsec in our adopted cosmology of $H_0 = 70\,{\rm km\,s^{-1}\,Mpc^{-1}}$ and $\Omega_\Lambda = 0.73$ and assuming a flat universe.

2 OBSERVATIONS AND DATA ANALYSIS

2.1 X-ray and radio imaging

Our *XMM–Newton* observations of 3C 469.1 were taken on 2008 September 29 and consist of 17.4 ks of EPIC-PN and 21.3 ks of EPIC-MOS data. Although the MOS data give roughly consistent results, they are much noisier and are not presented here. The EPIC-PN data were reduced using the standard *XMM–SAS* pipeline tasks EPCHAIN to give 443 ± 21 counts (of which 110 ± 4 are background) in the 0.3–10 keV band.

⋆Email: tlaskar@cfa.harvard.edu

[1] http://nedwww.ipac.caltech.edu

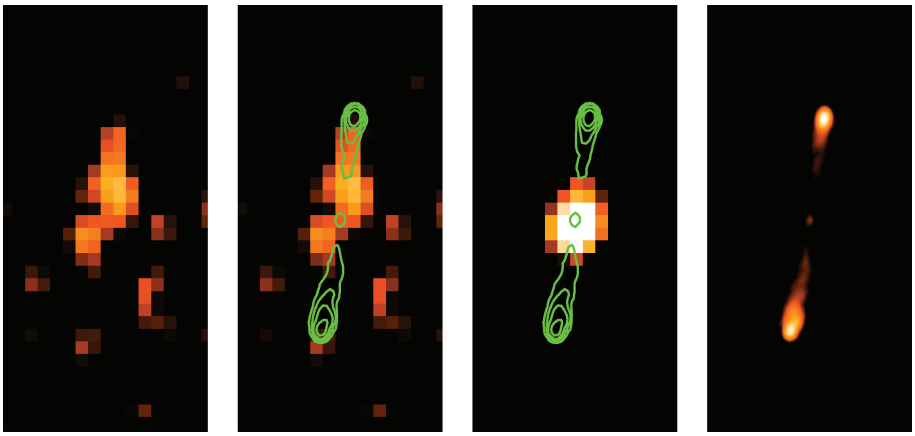

Figure 1. The panels show (from left to right) the *XMM*-pn image of 3C 469.1 below 1.2 keV, the same with 1.4 GHz radio contours overlaid, the pn image above 2 keV with the same radio contours and the 1.4 GHz radio image. The pixels in the X-ray images are 4.35 arcsec across. Each image is 150 arcsec (1.29 Mpc) high. All X-ray images (except Fig. 5) have been convolved with a Gaussian with a full width at half-maximum (FWHM) of 2 pixels, which is roughly the FWHM of the point spread function (PSF).

The source clearly shows extended emission at energies below 1.2 keV (Fig. 1). We estimate the detection significance of the entire extended emission to be 10σ and of the northernmost region of the quasi-linear structure to be 5σ. Above 2 keV, a central core remains, which is consistent with being a point source. The extended linear morphology of the soft X-ray emission precludes it from being due to hot cluster gas.

Radio data from all three targets came from the VLA archive. In the case of 3C 469.1, we used data from the A, B and C configurations (originally published by Kharb et al. 2008) to sample all the structure; for our other two targets, only B-configuration data were available. Interference was excised from the data and 3C 48 was used to set the absolute flux calibration; a number of rounds of phase self-calibration were performed, before a final iteration of phase and amplitude self-calibration. The final self-calibrated 1.5 GHz radio image for 3C 469.1 is shown in Fig. 1. The cospatial nature of the radio synchrotron emission compared with the soft X-rays from this source suggests a fundamental connection between the emitting particle populations within the lobes.

The flux density of the extended radio emission, after subtracting the contribution from the hotspots, is about 300 mJy, with the North and South radio lobes contributing 0.046 and 0.256 Jy, respectively. We note that the southern lobe is not detected in the soft X-ray image. A possible explanation for the extended emission is inverse-Compton scattering of infrared photons from the host galaxy (Brunetti, Setti & Comastri 1997) into the line of sight by plasma within the lobes, which would produce more intense X-rays in the lobe directed away from the observer. However, in order for the energy density of the nuclear photons to be comparable to that of the microwave background 200 kpc into the lobes, the nucleus would be required to have an infrared luminosity of $10^{48}\,\mathrm{erg\,s^{-1}}$, which is implausible. Therefore, it is more likely that the ICCMB is responsible for the observed X-ray flux. The discrepancy in the flux from the two lobes remains unresolved.

2.2 X-ray spectral analysis of 3C 469.1

The number of counts was insufficient to perform spectral fitting of the lobe and core regions separately (an attempt at fitting only the extended X-ray emission towards the North with a power law yielded a poorly constrained photon index of $\Gamma = 3.2^{+1.2}_{-1.6}$). Therefore spectra of the entire source were extracted, with regions on the same chip selected as background. The spectrum was binned to 20 counts bin^{-1} using GRPPHA and fitted in XSPEC v12.5.0 (Fig. 2).

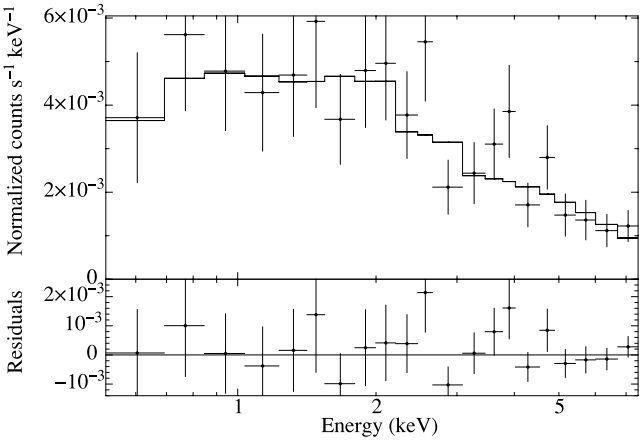

Figure 2. *XMM*-pn spectrum of 3C 469.1. The model fitted is shown in Fig. 3 and is described by equation (1) with the best-fitting parameters as shown in Table 1.

The model used was a set of power laws in photon energy for both the extended and core emissions, together absorbed photoelectrically by neutral hydrogen within our Galaxy, with allowance for additional soft-photon absorption within the host galaxy itself. Due to the poor constraints from the data, we assumed the two power-law indices to be the same. Mathematically, the model of the X-ray flux density as a function of the photon energy, E, is

$$M(E) = \mathrm{e}^{-N_{\mathrm{H}}^{1}\sigma(E)}\left(K_1 E^{-\Gamma_1} + \mathrm{e}^{-N_{\mathrm{H}}^{2}\sigma(E(1+z))}K_2 E^{-\Gamma_2}\right). \quad (1)$$

Here K_1 and K_2 are the normalizations of the emission at 1 keV from the lobes and the core, respectively, Γ_1 and Γ_2 are the corresponding photon indices (set equal), N_{H}^{1} is the absorbing column within our Galaxy along the line of sight to the source ($1.38 \times 10^{21}\,\mathrm{cm^{-2}}$; Kalberla et al. 2005), N_{H}^{2} is the extra absorbing column within the host galaxy, $\sigma(E)$ is the photoelectric cross-section (ignoring the Thomson scattering) and $z = 1.336$ is the redshift. The best-fitting model [$\chi^2 = 13.9$ for 17 degrees of freedom (d.o.f.)] is shown in Fig. 3 and the best-fitting values for this model are given in Table 1.

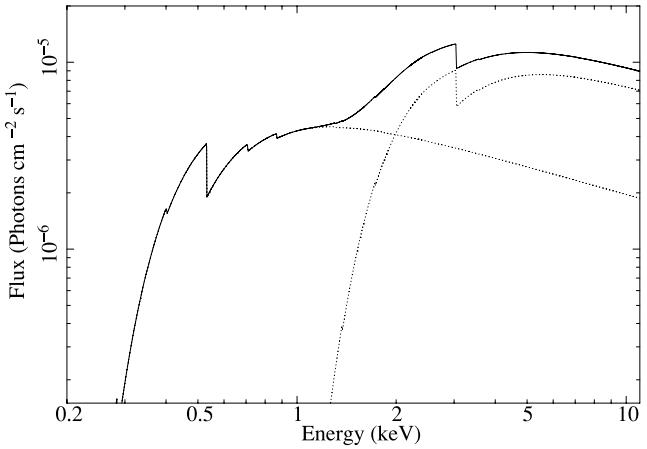

Figure 3. Best-fitting model for *XMM*-pn data for 3C 469.1. The model used (equation 1) is two absorbed power laws with the same photon index, with one power-law component further attenuated by an absorbing column (estimated at $29.4^{+18.3}_{-17.6} \times 10^{-22}$ cm^{-2} at 90 per cent confidence) within the host galaxy.

Table 1. The constraints on the parameters for the best-fitting model (equation 1).

Parameter	Value	Nominal error (90 per cent confidence)
$\Gamma_1 \equiv \Gamma_2$	1.5	0.6
$N_{\rm H}^2$	29	± 18
K_1	6.3	$^{+1.5}_{-1.7}$
K_2	24	$^{+48}_{-20}$

Note. $N_{\rm H}^2$ is the extra absorbing column within the host in 10^{22} cm^{-2} . K_1 and K_2 are the normalizations of the emission (in 10^{-6} keV^{-1} cm^{-2} s^{-1}) at 1 keV from the lobes and the core, respectively.

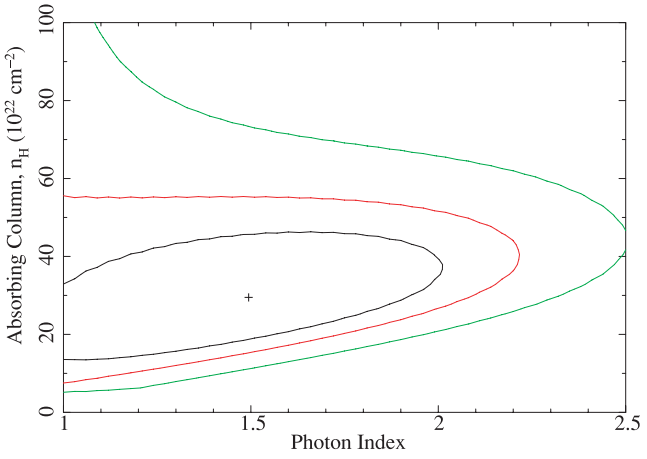

Figure 4. χ^2 contours at 68 per cent (innermost, black), 90 per cent (middle, red) and 99 per cent (outermost, green) confidence between the absorbing column in the host galaxy, $N_{\rm H}^2$, and the power-law photon index, Γ, for the best-fitting model for the 3C 469.1 spectrum.

The best-fitting model calls for a high absorption column in the nuclear component. A plot of the χ^2 contours of $N_{\rm H}^2$ versus Γ (Fig. 4) shows the extra absorption to be statistically significant. After correcting for Galactic absorption, the total luminosity in the rest frame of the source in the 2–10 keV band is 5.75×10^{44} erg s^{-1}, of which 3.25×10^{44} erg s^{-1} comes from the (absorbed) core component. The remaining luminosity of 2.5×10^{44} erg s^{-1}, corresponding to a flux density of 2.8×10^{-14} erg s^{-1} cm^{-2} (1.15 nJy for an X-ray bandwidth of $\sim$8 keV) at $z = 1.336$ from the unabsorbed (lobe) component, is comparable to the power in the X-ray-emitting lobes of the giant radio galaxy, 6C 0905+39 (1.5×10^{44} erg s^{-1}; Erlund et al. 2008). After correcting for both Galactic and host absorption, the 2–10 keV rest-frame luminosity of the nucleus is 9.8×10^{44} erg s^{-1}.

There are 22 photometric data points from 37 MHz to 14.9 GHz for 3C 469.1 in the NASA Extragalactic Database. A log–log plot of flux density versus frequency yields a straight line with a slope of -0.97 and a correlation coefficient of $r^2 = 0.98$. This implies an electron energy distribution proportional to $E^{-2.94}$, which is considerably steeper than the distribution [$E^{-(2\Gamma-1)} \propto E^{-2.0}$] implied by the X-ray spectra. However, our X-ray data only poorly constrain the photon spectral index and a value of $\Gamma = 1.97$, as expected from the radio photometry, is entirely within the (2σ) uncertainty (Fig. 4). Also, this fit does not take into account the core photon index separately, which may have a flatter spectrum than the lobes, forcing the overall best fit to lower values of Γ. Further, taking into account the noisy MOS data pushes up the value of Γ from 1.5 to 1.7. In what follows, we shall assume an electron energy distribution of $N_{\rm e}(E) \propto E^{-2.94}$ ($\Gamma = 1.97$) for this object.

3 DETERMINATION OF THE MAGNETIC FIELD

For an electron population with a power-law distribution of energies, $N_{\rm e}(E) \propto E^{-n}$, the synchrotron photons also follow a power-law spectrum with a spectral index, $\alpha = (n-1)/2$. The ratio of the flux density from inverse-Compton emission at $\nu_{\rm c}$ to the synchrotron flux density at $\nu_{\rm s}$ is given by (see e.g. Tucker 1977)

$$\frac{F_{\rm c}}{F_{\rm s}} = 2.47 \times 10^{-19} (5.23 \times 10^3)^{\alpha} \left(\frac{T}{1\,{\rm K}}\right)^{3+\alpha} \times \frac{b(n)}{a(n)} \left(\frac{B}{1\,{\rm G}}\right)^{-(\alpha+1)} \left(\frac{\nu_{\rm c}}{\nu_{\rm s}}\right)^{-\alpha}, \quad (2)$$

where B is the magnetic field strength in the radio-emitting lobes and T is the temperature of the CMB at the redshift of the source, and the constants $a(n)$ and $b(n)$ have been tabulated by Ginzburg & Syrovatskii (1965) and Tucker (1977), respectively.

Taking the flux density of the inverse-Compton emission to be the 2 to 10 keV (rest frame) X-ray flux density, the flux density of the synchrotron emission to be 300 mJy at 1505 MHz, $\alpha = 0.97$ and $h\nu_{\rm c} \approx 3$ keV yields a magnetic field of 12.5 μG. For comparison, taking $\alpha = 0.7$ in the above formula yields $B = 6.8$ μG, keeping all other values the same. It should be noted that this analysis requires the observed X-ray and radio fluxes to be cospatial. If the X-ray emission is more extended than the radio, then one must use in the above formulae only that part of the X-ray flux which overlays the radio and vice versa.

One can also determine the magnetic field by assuming the energy density in it to be the same as that of the electron population (see Longair 1994, equation 18.73). Taking the radio-emitting lobes of 3C 469.1 to be a cylindrical region 640 kpc long and 140 kpc in diameter and assuming a minimum Lorentz factor of the electron population, $\gamma_{\rm min} = 10^3$ gives an equipartition magnetic field of 9.0 μG. While this value is consistent with that determined from the X-ray and radio flux densities, the equipartition field depends on the

volume of the region ($B \propto V^{-3.97}$ for $\alpha = 0.97$), which is difficult to determine with the low spatial resolution of *XMM* and given the low number of counts. With the assumed volume stated above, we must have $\gamma_{\rm min} > 250$ for $\alpha \leq 0.97$ in order for the source to be in equipartition and to simultaneously explain the ICCMB X-ray flux. The volume emissivity in the ICCMB X-rays,

$$j(\nu) = 4.19 \times 10^{-40} T^3(z) b(n) N \left(\frac{2.1 \times 10^{10}}{\nu} T(z) \right)^{(n-1)/2}, \quad (3)$$

integrated over rest-frame energies from 2 to 10 keV and equated to the X-ray luminosity of the lobes, yields the number density of relativistic electrons to be $N/V = 2.2 \times 10^{-3}\,{\rm m}^{-3}$. Integrating the electron energies over a power-law distribution with index n between Lorentz factors $\gamma_{\rm min}$ and $\gamma_{\rm max}$ now allows for the determination of the total energy of the electrons responsible for the ICCMB. From the relation

$$\gamma \sim 1.89\sqrt{1+z} \left(\frac{\nu_{\rm R}}{1\,{\rm GHz}} \right)^{1/2} \left(\frac{B}{1\,\mu{\rm G}} \right)^{-1/2} 10^4, \quad (4)$$

the synchrotron emission at 14.9 GHz (Laing & Peacock 1980) corresponds to Lorentz factors of 3.2×10^4. Taking $\gamma_{\rm max}$ to be this value and assuming the electron energy spectrum to extend down to $\gamma_{\rm min} = 10^3$, the total energy in the plasma between $\gamma_{\rm min}$ and $\gamma_{\rm max}$ is 8.1×10^{59} erg, which is comparable to that found by Erlund et al. (2008) in the giant radio galaxy 6C 0905+39 and by Fabian et al. (2009) for HDF 130 in the Chandra Deep Field-North. The combined pressure produced by relativistic electrons and the magnetic field is $P/{\rm k_B} = 5.2 \times 10^4\,{\rm K\,cm^{-3}}$, which is comparable to that near the centre of a group of galaxies, but much larger than that of the intergalactic medium (IGM; $\sim$0.3 K cm^{-3}). Therefore, whether the lobes continue to expand depends on the environment.

4 MRC SOURCES

We also obtained observations of giant radio galaxies MRC 2216−206 ($z = 1.148$, linear size of 730 kpc; Kapahi et al. 1998) and MRC 0947−249 ($z = 0.854$, linear size of 530 kpc; Kapahi et al. 1998) with *XMM–Newton* on 2008 May 03 and May 10, respectively, with corresponding exposure times of 22.6 ks (8.8 ks)[2] and 17.0 ks (10 ks). In the 0.3–10.0 keV band, there are 361 ± 19 counts (of which 181 ± 6 are background, with 47 ± 19 soft[3] photons) for MRC 2216−206 and 195 ± 14 counts (of which 126 ± 6 are background, with 46 ± 11 soft photons) for MRC 0947−249. Whereas at higher energies the X-ray images are more consistent with being point-like sources near the location of the corresponding optical host galaxy, indicated by crosses (Figs 5 and 6), both sources show extended soft X-ray emission below 1.5 keV, which is plausibly due to the ICCMB.

We note that the soft emission in MRC 2216−206 appears to extend beyond the location of the south-east radio hotspot. This could indicate an earlier outburst resembling the double–double radio galaxy phenomenon (Schoenmakers et al. 2000) but with the outer/older lobes only being detectable via the ICCMB. However this extra emission, which consists of 30 counts in the 0.3–1.5 keV band, may also be due to a background AGN (at the corresponding flux level of $6 \times 10^{-15}\,{\rm erg\,s^{-1}\,cm^{-2}}$ in the 0.5–2.0 keV band for a photon index of $\Gamma = 2.0$ for these 30 counts, we estimate a 30 per cent probability of a coincident background source in the regions of interest around our three sources using the source counts of Hasinger et al. 2001). We did not include the region beyond the radio hotspots in our analysis.

[2]Good time remaining after filtering to remove flares and taking dead-time intervals into account.
[3]0.3–1.5 keV.

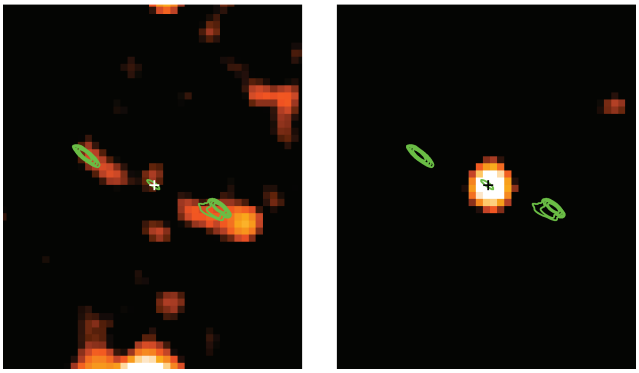

Figure 5. *XMM*-pn image MRC 2216−206 from 0.3 to 1.5 keV (left-hand panel) and 1.5 to 8.0 keV (from right-hand panel), with 4.86 GHz radio contours overlaid. Each panel is 222 arcsec high and 183 arcsec wide. The X-ray images have been convolved with a Gaussian with a FWHM of 3 pixels.

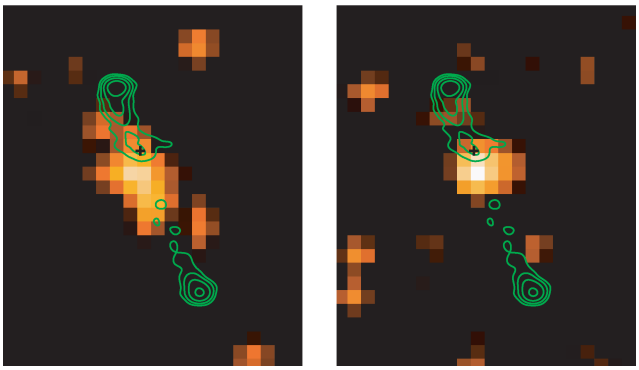

Figure 6. *XMM*-pn image of MRC 0947−249 from 0.3 to 1.5 keV (left-hand panel) and 1.5 to 8.0 keV (right-hand panel), with 4.86 GHz radio contours overlaid. Each panel is 114 arcsec high and 95 arcsec wide.

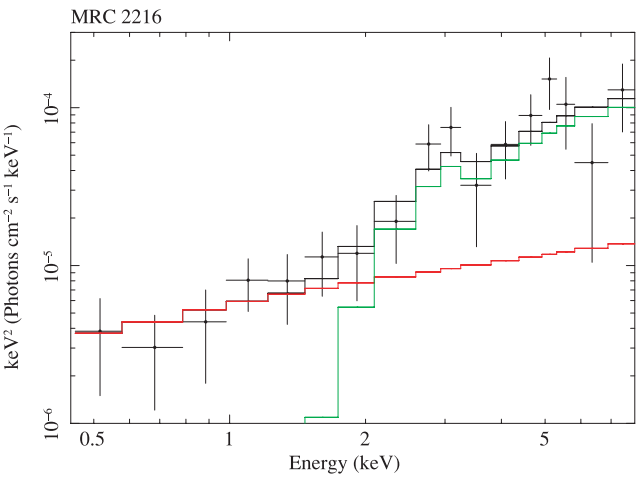

Figure 7. Unfolded *XMM*-pn spectrum of MRC 2216−206. The model fitted is described by equation (1). Note that the y-axis is equivalent to νF_ν. The red line depicts the extended ICCMB component and the green line the absorbed nuclear component.

Table 2. Observed X-ray luminosities for the sources in this paper.

Source	RA (J2000)	Dec. (J2000)	z	Count rate (cts s^{-1})	N_H (10^{21} cm^{-2})	Unabsorbed flux	L_{44}	$\mathcal{E}_e$
3C 469.1	$23^h55^m23^s.3$	$+79^d55^m20^s$	1.336	1.93×10^{-2}	1.38	3.58	2.56	8.1
MRC 2216−206	$22^h19^m44^s.2$	$-20^d21^m31^s$	1.148	2.09×10^{-2}	0.25	2.93	1.63	5.7
MRC 0947−249	$09^h49^m52^s.9$	$-25^d11^m40^s$	0.854	4.50×10^{-3}	0.46	1.22	0.45	2.9

Note. N_H is the Galactic neutral hydrogen column density along the line of sight, calculated using PIMMS. Columns 7 and 8 show the observed X-ray flux in 10^{-14} erg cm^{-2} s^{-1} and the X-ray luminosity in 10^{44} erg s^{-1} (2-10 keV, rest frame) respectively, both corrected for Galactic absorption. Column 9 shows the total energy in relativistic electrons in 10^{59} erg, estimated using equation (3) for 3C 469.1 and equation (5) for the MRC sources. For 3C 469.1 and MRC 2216 the quoted values of flux, luminosity and energy are for the lobe component as determined from spectrum-fitting, while for MRC 0947 they have been calculated from the observed soft (0.3–1.5 keV) X-ray count rate of 4.6×10^{-3} s^{-1} using PIMMS.

Spectral analysis of MRC 2216−206 was carried out exactly as for 3C 469.1, since a single-component power-law fit gave an unphysically hard photon index of $\Gamma = 0.5 \pm 0.35$. The two-component model yielded an extra host absorption of $3.8 \pm 1.8 \times 10^{23}$ cm^{-2} and a best-fitting energy index, $\Gamma = 1.6^{+0.5}_{-0.4}$, consistent with a radio synchrotron index of $\alpha = 1$ derived from NED archival radio photometry. The unabsorbed 2–10 keV luminosity of the nucleus is 1.3×10^{45} erg s^{-1}. The unfolded spectrum, along with the best-fitting model and residuals, is shown in Fig. 7.

If we assume that the observed X-rays are ICCMB photons, we can follow equation 4 of Erlund et al. (2006) to estimate the total energy in relativistic particles from the X-ray flux alone:

$$\mathcal{E}_e = \frac{3}{4}\frac{L_{44}}{\gamma_e(1+z)^4}10^{64}\ \mathrm{erg}, \quad (5)$$

where L_{44} is the X-ray luminosity in 10^{44} erg s^{-1} and γ_e is the typical Lorentz factor of the electrons up-scattering the CMB to X-rays. Setting $\gamma_e = 10^3$ gives $\mathcal{E}_e = 5.7 \times 10^{59}$ erg for MRC 2216−206. This is a lower limit to the total particle energy in the lobes of this object.

There were insufficient counts to fit the spectrum of MRC 0947−249. Instead, the soft-photon count rate (4.6×10^{-3} s^{-1}) was used along with a power-law model and an assumed photon energy index of $\Gamma = 2.0$ to estimate the flux of the extended emission with PIMMS.[4] The luminosity and total energy in relativistic particles thus determined are given in Table 2, together with the corresponding values for 3C 469.1 and MRC 2216−206 determined from spectrum fitting.

5 CONCLUSIONS

We have detected extended X-ray emission in the giant FR II radio galaxy, 3C 469.1, which extends up to the northern radio hotspot. The spectrum is well fitted ($\chi^2 = 13.9$ for 17 d.o.f.) by a power law with a photon index consistent with the radio spectral index. Energy equipartition arguments agree with the magnetic field estimates made for 3C 469.1 based on the X-ray flux inferred to be the ICCMB, provided γ_{min} is in excess of 250.

Further, we have presented *XMM* images of two more radio galaxies at cosmological distances, which show extended X-ray emission attributable to the ICCMB. The nuclei of all these sources have quasar-like luminosities and appear to be heavily absorbed powerful AGN, while the radio-emitting lobes have relativistic particles with similar total energies, ranging between 3 and 6×10^{59} erg. These values are enhanced if there is significant energy in protons.

It appears that ICCMB X-ray emission is indeed observable from giant radio galaxies at redshift $z \sim 1$. However, the cospatial nature of the X-rays with radio observations remains an important caveat in the determination of the magnetic field. Further observations of these sources with the finer PSF of *Chandra* would help resolve this issue and observations with a greater signal-to-noise ratio would provide better constraints on the X-ray spectral index, which is essential for accurate determinations of γ_{min} and the establishment of the nature of the low-energy turnover in aged AGN lobes.

ACKNOWLEDGMENTS

ACF and KMB thank The Royal Society for support. This work was supported by the Cavendish Laboratory, Cambridge, and a scholarship from the Jawaharlal Nehru Memorial Trust and the Cambridge Commonwealth Trust.

REFERENCES

Blundell K. M., Fabian A. C., Crawford C. S., Erlund M. C., Celotti A., 2006, ApJ, 644, L13
Brunetti G., Setti G., Comastri A., 1997, A&A, 325, 898
Croston J. H., Hardcastle M. J., Harris D. E., Belsole E., Birkinshaw M., Worrall D. M., 2005, ApJ, 626, 733
Erlund M. C., Fabian A. C., Blundell K. M., Celotti A., Crawford C. S., 2006, MNRAS, 371, 29
Erlund M., Fabian A. C., Blundell K. M., 2008, MNRAS, 386, 1774
Fabian A. C., Sanders J. S., Crawford C. S., Ettori S., 2003, MNRAS, 341, 729
Fabian A. C., Chapman S., Casey C. M., Bauer F., Blundell K. M., 2009, MNRAS, 395, L67
Fanaroff B. L., Riley J. M., 1974, MNRAS, 167, 31P
Ginzburg V. L., Syrovatskii S. I., 1965, ARA&A, 3, 297
Hasinger G. et al., 2001, A&A, 365, L45
Johnson O., Almaini O., Best P. N., Dunlop J., 2007, MNRAS, 376, 151
Kalberla P. M. W., Burton W. B., Hartmann D., Arnal E. M., Bajaja E., Morras R., Pöppel W. G. L., 2005, A&A, 440, 775
Kapahi V. K., Athreya R. M., van Breugel W., McCarthy P. J., Subrahmanya C. R., 1998, ApJS, 118, 275
Kharb P., O'Dea C. P., Baum S. A., Daly R. A., Mory M. P., Donahue M., Guerra E. J., 2008, ApJS, 174, 74
Laing R. A., Peacock J. A., 1980, MNRAS, 190, 903
Longair M. S., 1994, High Energy Astrophysics, Stars, the Galaxy and the Interstellar Medium, Vol. 2. Cambridge Univ. Press, Cambridge
Schoenmakers A. P., de Bruyn A. G., Röttgering H. J. A., van der Laan H., Kaiser C. R., 2000, MNRAS, 315, 371
Schwartz D. A., 2002, ApJ, 569, L23
Tucker W. H., 1977, Radiation Processes in Astrophysics. MIT Press, Cambridge, MA

[4]http://heasarc.nasa.gov/Tools/w3pimms.html

This paper has been typeset from a TEX/LATEX file prepared by the author.